Supporting Information for: Mapping the multi-step mechanism of a photoredox catalysed atom-transfer radical polymerization reaction by direct observation of the reactive intermediates

Luke Lewis-Borrell[1‡], Mahima Sneha[1‡], Aditi Bhattacherjee[a‡], Ian P. Clark[2] and Andrew J. Orr-Ewing[1]*

[1]School of Chemistry, University of Bristol, Cantock's Close, Bristol BS8 1TS, UK

[2]Central Laser Facility, Research Complex at Harwell, Science and Technology Facilities Council, Rutherford Appleton Laboratory, Harwell Oxford, Didcot, Oxfordshire, OX11 0QX, UK

[a]: Present address: AMOLF, Science Park 104, 1098 XG Amsterdam, The Netherlands

Contents

General Information 2
Synthesis 3
(i) 5,10-dihydrophenazine 3
(ii) 5,10-di(naphthalen-1-yl)-5,10-dihydrophenazine (PCBN) 3
Steady State Spectra 3
Data Collection 3
FTIR Spectra 4
(i) 5,10-di(naphthalen-1-yl)-5,10-dihydrophenazine (PCBN) 4
(ii) Methyl 2-bromopropionate (MBP) 5
(iii) PCBN oxidation with $FeCl_3$ 6
Electronic Spectra 6
(i) PCBN UV-Vis 6
(ii) PCBN Emission 7
Transient Spectra 7
Data Collection 7
(i) University of Bristol Ultrafast Laser System 7
(ii) STFC Rutherford Appleton Laboratory: LIFEtime Laser System 8
(iii) Sample Preparation and Flow system 8
TA data 10
(i) PCBN in toluene 10
(ii) PCBN in DMF 10
(iii) PCBN in DCM 11
(iv) Triplet state formation in DCM 11
(v) PCBN with MBP in DMF 12
(vi) PCBN TVAS in toluene-d_8 13

(vii) PCBN TVAS in DMF 13
TEAS Data Fitting 13
(i) PCBN lifetime data 13
(ii) PCBN and MBP data 16
Kinetic Analysis 18
Kinetics of the electron transfer between photoexcited PCBN and MBP 18
(i) Kinetics for the rise of the $^2MP^{\bullet}(D_0)$ absorption band observed at 1660 cm^{-1} in TVA spectra obtained for a solution of PCBN (2.1 mM) and MBP (various concentrations from 0.2 - 1.1 M) in DCM following 370-nm excitation. 18
(ii) Kinetics for the rise of $^2MP^{\bullet}(D_0)$ absorption band observed at 1660 cm^{-1} in TVA spectra obtained for a solution of PCBN (2.1 mM) and MBP (various concentrations from 0.2 - 1.1 M) in toluene-d_8 following 370-nm excitation. 19
(iii) *Kinetics of PCBN S_1 decay derived from analysis of TEA spectra obtained for a solution of PCBN (2.1 mM) and MBP (various concentrations from 0.2 – 1.1 M) in DMF following 370-nm excitation* 20
(iv) N_2 purged vs un-purged decay of the $^2MP^{\bullet}(D_0)$ absorption band observed at 1660 cm^{-1} in TVA spectra obtained for a solution of PCBN (2.1 mM) and MBP. 21
Smoluchowski vs single exponential kinetic fitting 21
Calculations for $\Delta(\Delta PETG)$ 23
Kinetic Models 24
(i) Kinetic model for PCBN* / MBP electron transfer reactions for the analysis of PCBN*(S_1) decay rates 24
(ii) Kinetic model for the propagation reaction step 24
Computational Methodology 25
Excited State Calculations 25
References 25

General Information

For synthesis of 5,10-di(naphthalen-1-yl)-5,10-dihydrophenazine, anhydrous solvents were commercially supplied or provided by the communal stills of the School of Chemistry, University of Bristol, and were dried using a purification column composed of activated alumina and stored over thoroughly dried 3 Å molecular sieves. All other solvents were bought through Sigma-Aldrich. 2-Dicyclohexylphosphino-2,6-diisopropoxybiphenyl (RuPhos) and Chloro-(2- Dicyclohexylphosphino-2,6-diisopropoxy-1,1-biphenyl) [2-(2-aminoethyl)phenyl] palladium(II) - methyl-t-butyl ether adduct (RuPhos precatalyst) were bought from Sigma-Aldrich and stored under nitrogen atmosphere. All other reagents were used as received.

^{1}H NMR spectra were recorded using Jeol ECS 400 MHz and Varian VNMR 400 MHz spectrometers. Chemical shifts (δ) are given in parts per million (ppm). The ^{1}H NMR spectra are reported as follows: ppm (multiplicity, integration).

For transient spectroscopy experiments, all solvents were spectroscopic grade or anhydrous in the case of dichloromethane (DCM) or N,N-dimethylformamide (DMF). The methyl 2-bromopropionate (MBP) and isoprene used were purchased from Sigma-Aldrich. All chemicals were degassed with nitrogen for 30-40 minutes prior to use in experiments.

Synthesis

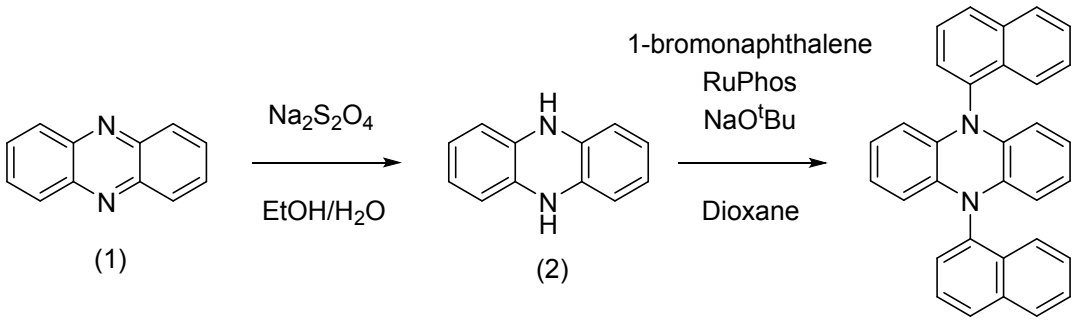

(i) 5,10-dihydrophenazine

A conical flask was charged with phenazine **1** (2.0 g, 11 mmol) in EtOH (50 mL) and heated to reflux. With stirring, a solution of $Na_2S_2O_4$ (23.3 g, 134 mmol) in water (200 mL) was then added over a period of 5 min, leading to the formation of a pale green precipitate after 10 min. The crude solid was isolated via vacuum filtration, washed thoroughly with water and dried in vacuo to afford 5,10-dihydrophenazine **2** (1.73 g, 10.4 mmol, 94 %) as a pale green powder. No further purification was performed on **2** and **3** was synthesised immediately after exposing **2** to the atmosphere.

(ii) 5,10-di(naphthalen-1-yl)-5,10-dihydrophenazine (PCBN)

The photocatalyst PCBN **3** was synthesised via a Buchwald-Hartwig coupling reaction. An oven-dried round-bottom flask was charged with a magnetic stirrer bar, **2** (0.50 g, 2.7 mmol), NaO^{t}Bu (2.11 g, 22.0 mmol), RuPhos (103 mg, 0.22 mmol), RuPhos precatalyst (180 mg, 0.22 mmol), 1-bromonapthalene (4.55 g, 22 mmol) and 1,4-dioxane (10 ml) and heated to 110 °C under an atmosphere of nitrogen. After 16 hr the solution had turned green and a yellow precipitate had been formed. The reaction mixture was diluted in DCM (200 ml) and water (200 ml), causing further precipitation so the solid was isolated and washed with hexane and kept to the side. The remaining DCM solution was washed with water again (2 x 200 ml), the organic layer was dried over $MgSO_4$, and vacuum filtered. Finally, the DCM was removed under vacuum until precipitation could be seen, hexane was then added dropwise to induce further precipitation. The precipitate was collected as a bright yellow solid and combined with the previously isolated precipitate as both were determined to be product (1.05 g, 2.41 mmol, 43 %). Characterization was confirmed by comparison with previously reported values.[1]

^{1}H NMR (d_8-toluene, 400 MHz) δ 8.64 – 8.54 (m, 2H), 7.73 – 7.63 (m, 4H), 7.47 (m, 2H), 7.33 – 7.22 (m, 6H), 6.12 – 6.03 (dd, 4H), 5.70 – 5.63 (dd, 4H).

Steady State Spectra

Data Collection

Steady-State Spectroscopy. All steady-state UV-Vis absorption spectra reported herein were obtained with a Thermo Scientific Genesys 10S spectrophotometer. The solutions were contained in a stainless-steel Harrick cell with CaF_2 windows and sample path length of 380 µm for both UV and

IR measurements. Solutions were prepared to a concentration such that they exhibited an absorbance of 0.05 < A(λ_{max}) < 0.5 OD at the excitation wavelength λ_{max}. Emission spectra were measured with a PerkinEmer LS-45 Luminescence spectrometer with 10-nm excitation and 20-nm emission slits. Emission spectra were obtained using glass cuvettes of path length 1 cm. FTIR spectra were recorded on a PerkinElmer Spectrum-Two spectrometer.

FTIR Spectra

(i) 5,10-di(naphthalen-1-yl)-5,10-dihydrophenazine (PCBN)

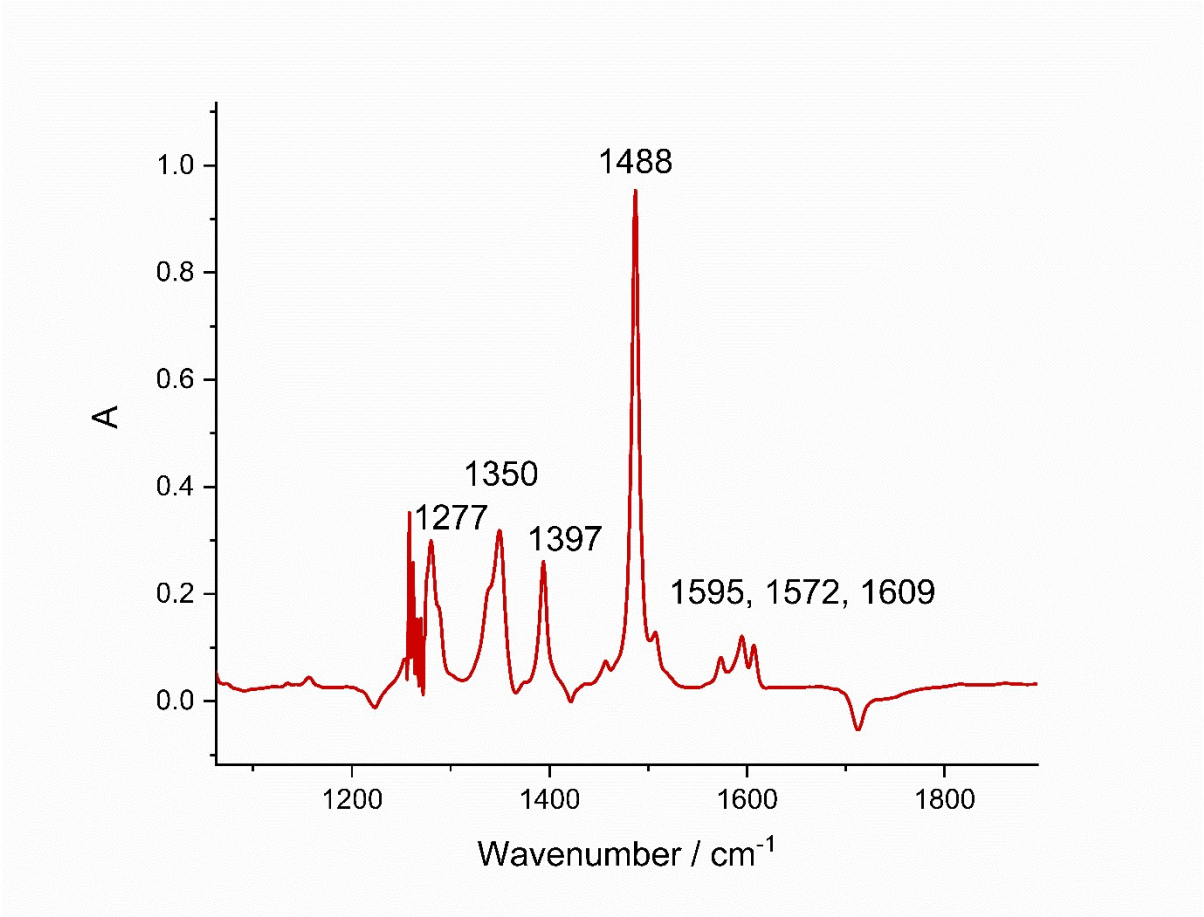

Figure S1. FTIR absorption spectrum for 5,10-di(naphthalen-1-yl)-5,10-dihydrophenazine (PCBN, 21 mM, 380 µm path length) taken in DCM. Solvent absorption bands have been subtracted from the spectrum. All the important peaks are labelled.

(ii) Methyl 2-bromopropionate (MBP)

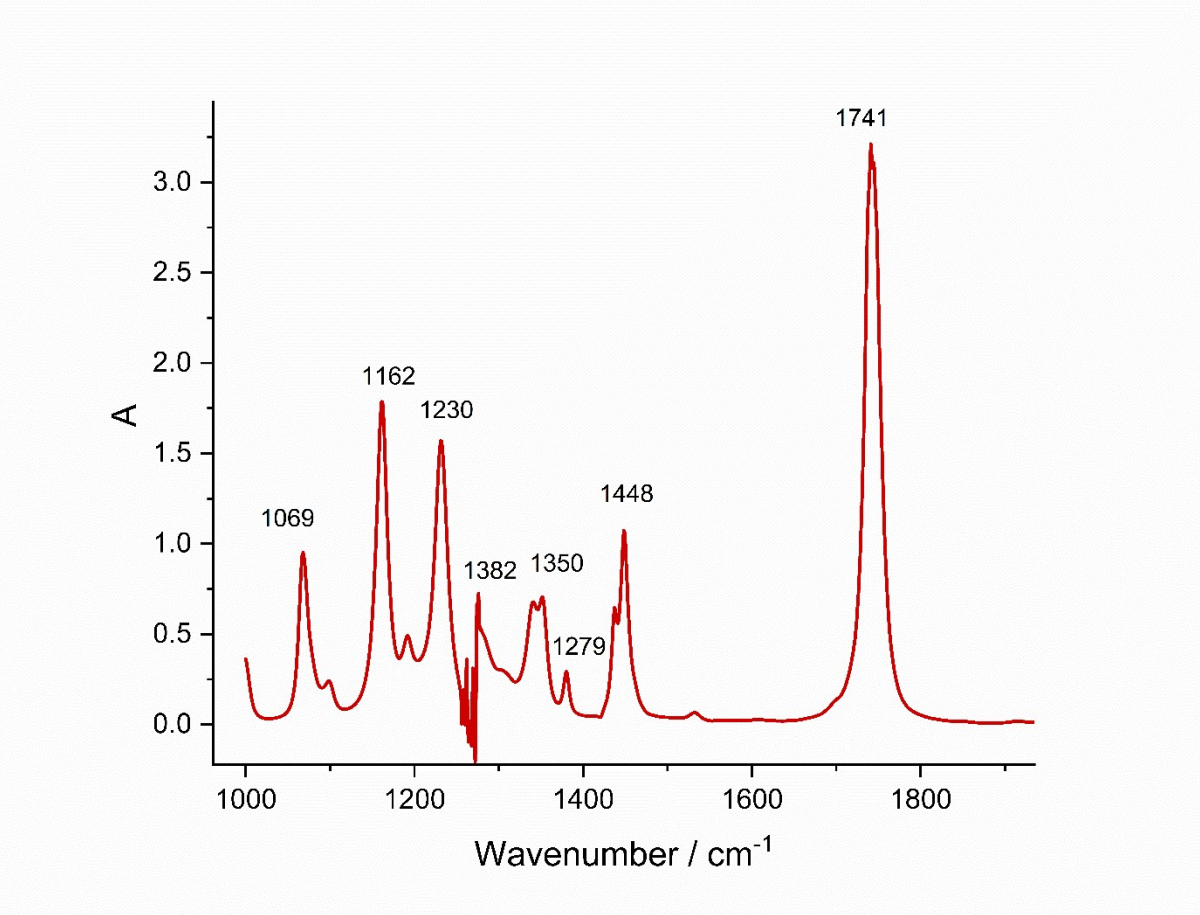

Figure S2. FTIR spectrum for methyl 2-bromopropionate(21 mM, 380 µm path length) in DCM. Solvent absorption bands have been subtracted from the spectrum. All the important peaks are labelled.

(iii) PCBN oxidation with $FeCl_3$

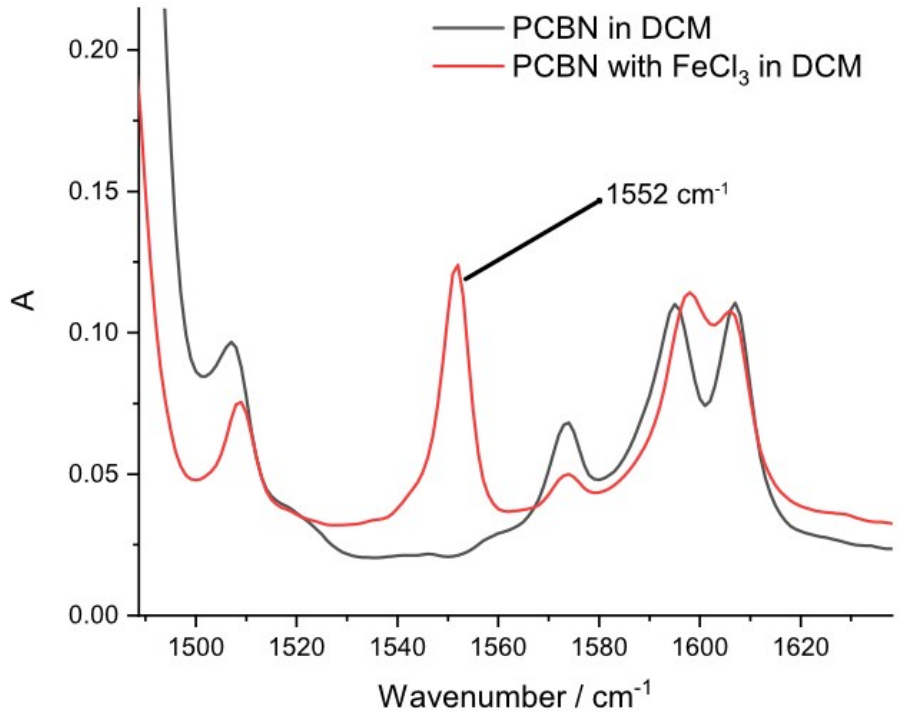

Figure S3. FTIR spectra of 21 mM PCBN in DCM without (black) and with (red) 3 equivalents of $FeCl_3$ (pathlength 300 µm). The latter spectrum shows a peak at 1552 cm^{-1} assigned to the $PCBN^{+\bullet}$ radical cation formed by oxidation.

Electronic Spectra

(i) PCBN UV-Vis

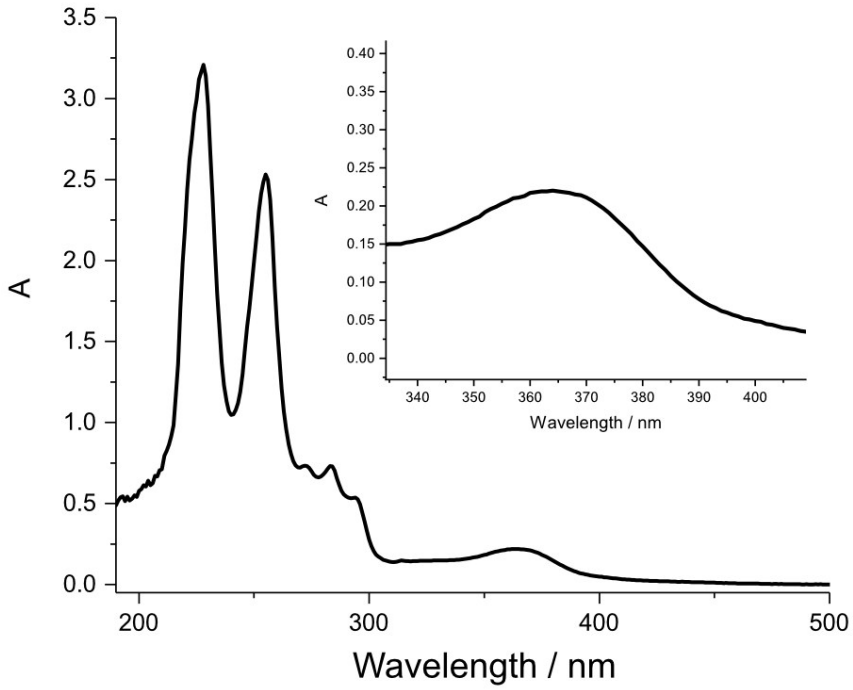

Figure S4. UV-Vis absorption spectrum of 5,10-di(naphthalen-1-yl)-5,10-dihydrophenazine (PCBN, 2.1 mM, 380 µm) in DCM, with an expanded view of the near-UV region above 340 nm shown in the inset.

(ii) PCBN Emission

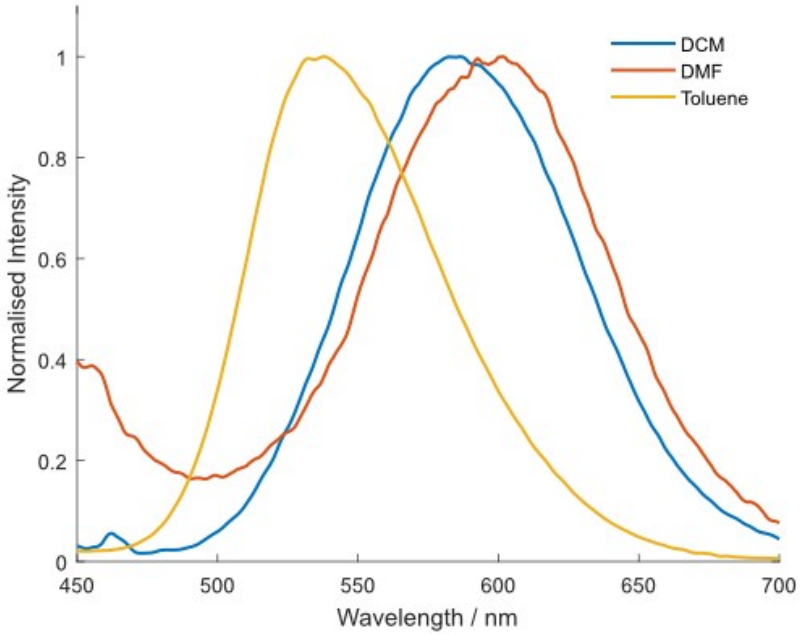

Figure S5. Emission spectra for 5,10-di(naphthalen-1-yl)-5,10-dihydrophenazine excited at 370 nm. Spectra were measured for PCBN in toluene, DCM and DMF and are normalised to a maximum emission intensity of 1.0.

Transient Spectra

Data Collection

Experiments reported here were performed in the ultrafast laser laboratory in the School of Chemistry, University of Bristol and at the LIFEtime facility at the STFC Rutherford Appleton Laboratory's Central Laser Facility. The transient spectroscopic data reported were analysed using the custom labVIEW program KOALA.[2]

(i) University of Bristol Ultrafast Laser System

The ultrafast laser system at the University of Bristol was used to record transient electronic absorption spectra covering the early time dynamics of the reaction (time delays spanning 100 fs to 1.3 ns). The system is described in detail elsewhere and only details pertaining to the experiment are mentioned here.[2] Briefly, an ultrafast Coherent Legend Elite HE+ regenerative amplifier, operating at 1 kHz and configured to produce 40 fs duration pulses at 800 nm (output power 5W) seeds two Coherent OPerA Solo optical parametric amplifiers (OPAs). These OPAs generate UV and mid-IR beams via various nonlinear frequency-mixing schemes combining the OPA signal and idler, and 800-nm pump beams. For the experiments reported here, only one OPA is required to generate the pump beam at 370 nm using the fourth harmonic of the OPA signal beam. A lower energy portion of the 800-nm pump laser beam (100 μJ/pulse) generates a white light continuum (WLC) probe by focusing (using a CaF_2 lens of focal length f = 200 mm) into a 2-mm thick CaF_2 window which is continuously rastered to avoid thermal damage. An off-axis parabolic mirror (f = 100 mm) collimates the resulting WLC probe, which spans wavelengths from ~330 nm to >700 nm.

The WLC probe pulse is reflectively focused into the sample using an f = 75 mm concave aluminum mirror (to avoid achromatic aberrations) to obtain a ~50 μm beam diameter. The pump beam is polarized at magic angle (54.7 degrees) relative to the WLC probe and is focused loosely using a f = 35 mm lens to ensure uniform excitation of the sample in the probed region. The temporal delay (Δt) between the pump and WLC probe beams is controlled by changing the path length of the pump beam with an aluminum retro-reflector (PLX) mounted on a motorized 220 mm delay stage (Thorlabs, DDS220/M), providing a maximum delay of Δt = 1.3 ns. The maximum pump power used is 300 nJ/pulse at the sample to avoid multi-photon excitations. A non-collinear overlap of the pump and probe beams on the sample allows separation after the sample, and the transmitted WLC beam is focused into a spectrograph (Andor, Shamrock 163) fitted with a 1024-element photodiode array (Entwicklungs-büro Stresing). An optical chopper wheel operating at 500 Hz (Thorlabs, MC2000) is used to block every other pump beam to compare pump-on and pump-off spectra at each time delay. The spectra are processed to obtain differential absorbance:

$$\Delta A(t) = -\log\left(\frac{I_{pump\ on}}{I_{pump\ off}}\right)$$

Typically, the spectra are averaged for two seconds with three repeat cycles of 88 timepoints. The spectrometer is calibrated against the electronic spectrum of Holmium oxide.

(ii) STFC Rutherford Appleton Laboratory: LIFEtime Laser System

Transient vibrational absorption spectra were recorded using the LIFEtime laser system at the STFC Rutherford Appleton Laboratory, allowing an extended range of measurement times from 200 fs to 1 ms.[3, 4] The details of the laser system are described in reference [4]. Briefly, a single Yb:KGW ultrafast oscillator seeds two Yb:KGW amplifiers (Light Conversion Ltd., Pharos, 100 kHz, 15 W, 260

fs output pulses and Pharos, 100 kHz, 6W, 180 fs output pulses). The higher power amplifier is used to generate a single UV-Vis pump, while the 6W amplifier drives two OPAs with DFG units to generate two mid-IR probe beams. In each case Light Conversion Orpheus OPAs are used. The 370-nm UV pump beam is collimated and passed along a 0-12 ns optical delay stage before focusing (120-150 μm diameter) at the sample. The laser's pulse-picker is used to reduce the repletion-rate of this pump beam down to 1 kHz.

The dual mid-IR probe beams (each with bandwidth ~200 cm^{-1}) can be individually tuned to different mid-IR regions and for this experiment are centred in the aromatic ring mode (1400-1600 cm^{-1}) and CO stretch (1550-1750 cm^{-1}) regions. Both probe beams operate at a repetition rate of 100 kHz. The two probe beams are collimated and then focused (50-75 μm diameter) by a gold off-axis parabolic mirror (7.5 cm focal length) onto the sample. The pump and probe beams are spatially overlapped at the sample with relative polarizations set at magic angle. The probe beams are dispersed into two separate 128-element MCT detector arrays (Infrared Associates). A pixel-to-wavenumber calibration is applied using a spectrum of polystyrene. The last probe spectrum in a 100 probe pulse sequence for each UV pump pulse is used for the pump-off measurement.

The pump power is 150-300 nJ/pulse at the sample and both mid-IR probes are set at ~0.05 μJ/pulse. Data is collected in a time-resolved multiple probe fashion as described in reference [3], using 112 timepoints between 1 ps and 9 μs, and 10 μs (the probe amplifier repetition period). Three-second averaging with three repeat cycles are performed for each time delay.

(iii) Sample Preparation and Flow system

Solutions are prepared to desired concentrations of various reagents in a glass vial, or in a Duran bottle sealed flow system as shown in **Figure S6**. For the photocatalyst lifetime measurements, a 2.1 mM solution of PCBN is made in 10 mL of DCM, DMF or toluene-d_8/toluene. For concentration-dependent MBP and MBP/Isoprene experiments, increasing amounts of MBP or Isoprene are added to the catalyst solution using a syringe. To avoid oxygen contamination, the solutions are prepared using degassed solvents and are thoroughly purged with nitrogen. The headspace of the bottle is filled with nitrogen prior to sealing. Unfortunately, with the sample flow system shown in **figure S6**, it is difficult to exclude oxygen leaks completely over the course of the experiment. The bottle is connected via PTFE tubing to a Harrick cell comprising two CaF_2 windows (1.5 mm thick) separated by a teflon spacer of thickness 100-200 μm (which set the pathlength) and sealed by Kalrez O-rings. The solutions continuously flow through the cell, with circulation driven by a peristaltic pump. The continuous flow ensures that consecutive pump and probe pulses sample fresh volume of solution. The cell is also rastered in the xy-plane perpendicular to the direction of beam propagation to avoid accumulation of photoproducts on the windows.

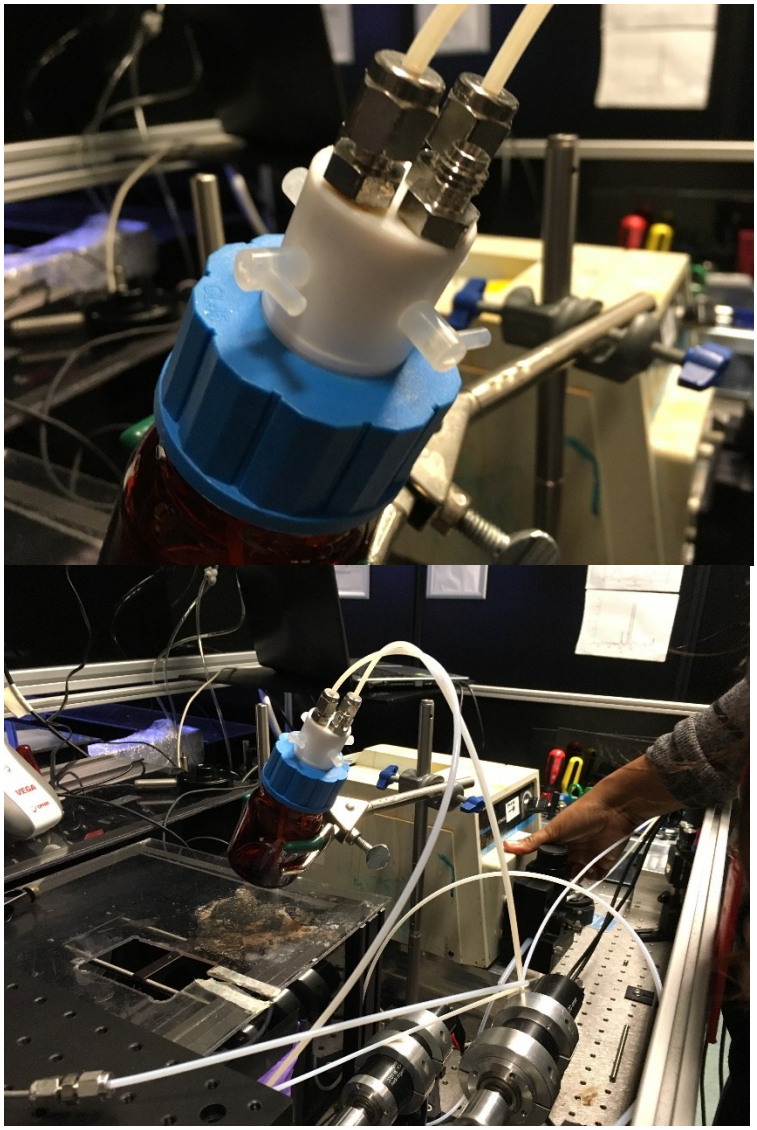

Figure S6. Sample flow system used for TVAS experiments at the LIFEtime Facility.

TA data

(i) PCBN in toluene

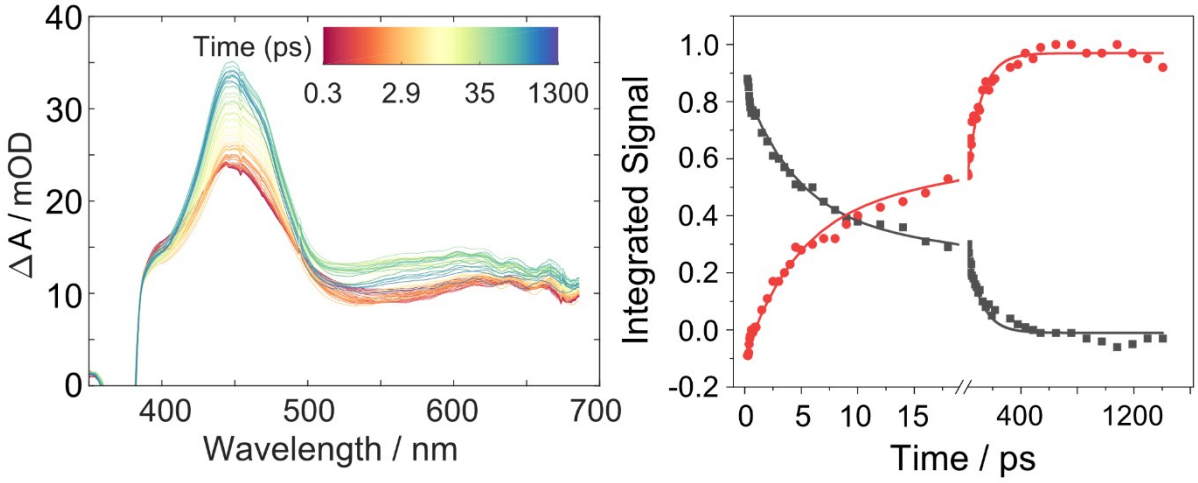

Figure S7. TEAS measurements over the wavelength range 350-700 nm following pulsed excitation of a PCBN / toluene solution at 370 nm. (a) TEA spectra obtained at time delays from 0 – 1300 ps (with the dip at wavelengths below 400 nm caused by PCBN ground-state absorption); (b) corresponding kinetic traces obtained by spectral decomposition (see text). Note the break in the time axis to highlight early and later time kinetic components. The solid lines are global fits with biexponential time constants of τ_1=4.7 ± 0.3 ps and τ_2=91 ± 5 ps. Respective fit amplitudes for the red kinetic trace are A_1=0.49 ± 0.02 and A_2=0.37 ± 0.02. The kinetic analysis is discussed further in the main text.

(ii) PCBN in DMF

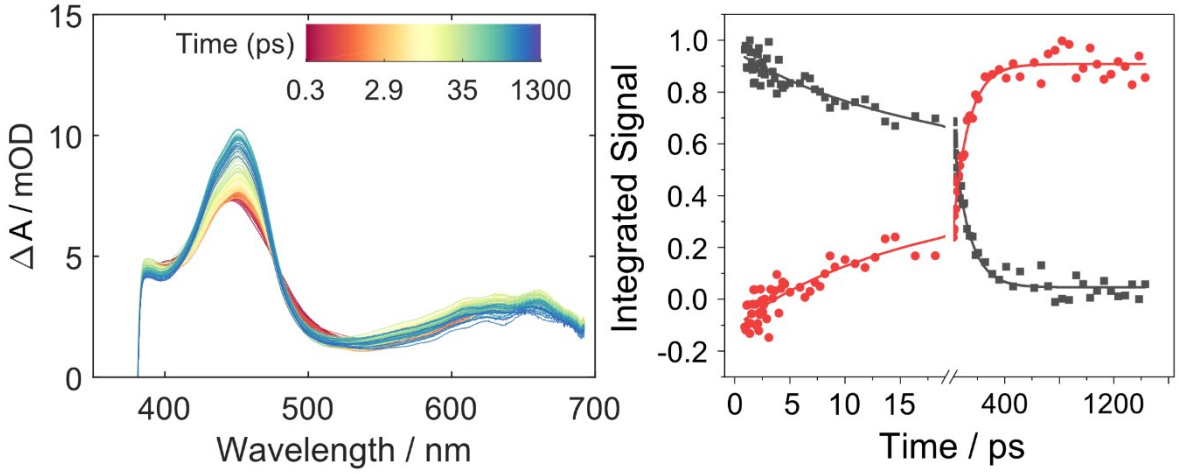

Figure S8. TEAS measurement over the wavelength range 350-700 nm following pulsed excitation of a PCBN / DMF solution at 370 nm. (a) TEA spectra for PCBN (2.1 mM) in DMF (b) The corresponding kinetic traces obtained by spectral decomposition. Note the break in the time axis to highlight early and later time kinetic components. The solid lines are global fits with biexponential time constants of τ_1=10.4 ± 2.6 ps and τ_2=111 ± 8 ps. Respective fit amplitudes for the red kinetic trace are A_1=0.19 ± 0.03 and A_2=0.72 ± 0.03.

(iii) PCBN in DCM

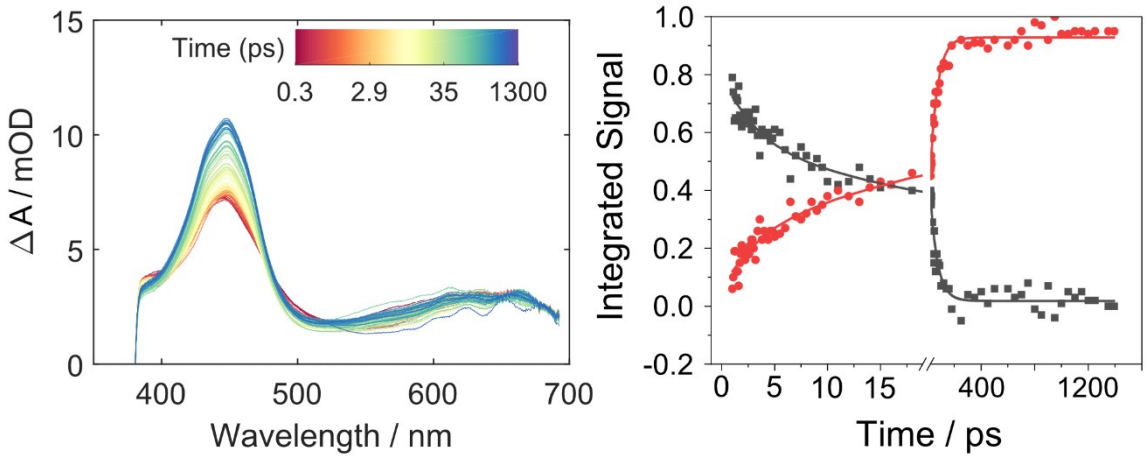

Figure S9. TEAS measurement over the wavelength range 350-700nm following pulsed excitation of a PCBN / DCM solution at 370 nm. (a) TEA spectra for PCBN (2.1 mM) in DCM (b) The corresponding kinetic traces obtained by spectral decomposition. Note the break in the time axis to highlight early and later time kinetic components. The solid lines are global fits with biexponential time constants of τ_1=3.4 ± 0.7 ps and τ_2=54.6 ± 3.3 ps. Respective fit amplitudes for the red kinetic trace are A_1=0.25 ± 0.03 and A_2=0.53 ± 0.02.

(iv) Triplet state formation in DCM

Analysis of the ground state bleach (GSB) feature evident in TVAS measurements for a 2.1 mM PCBN solution in DCM at time delays from 0 to 100 ns shows there is ~80% ground-state recovery (with a time constant of 15 ns) but that ~20% of the excited state population does not return to the ground state. Measurements extended to longer times reveal a secondary ground-state recovery pathway for this 20% fraction on a microsecond time scale. A fit of the time-dependent GSB intensities measured at delays from 100 ns to 9 µs with a single exponential function gives a time constant of 0.5 µs (**Figure S10**). We discount any electron transfer to the solvent (DCM) as contributing to this delayed ground-state recovery because we do not see evidence for the $PCBN^{\bullet+}$ absorption band known to arise at 1552 cm^{-1} (see Figure S3). Thus, the final decay is attributed to a triplet state (T_1), although we do not see any transient absorption features associated with the T_1 state in our IR probe spectral range.

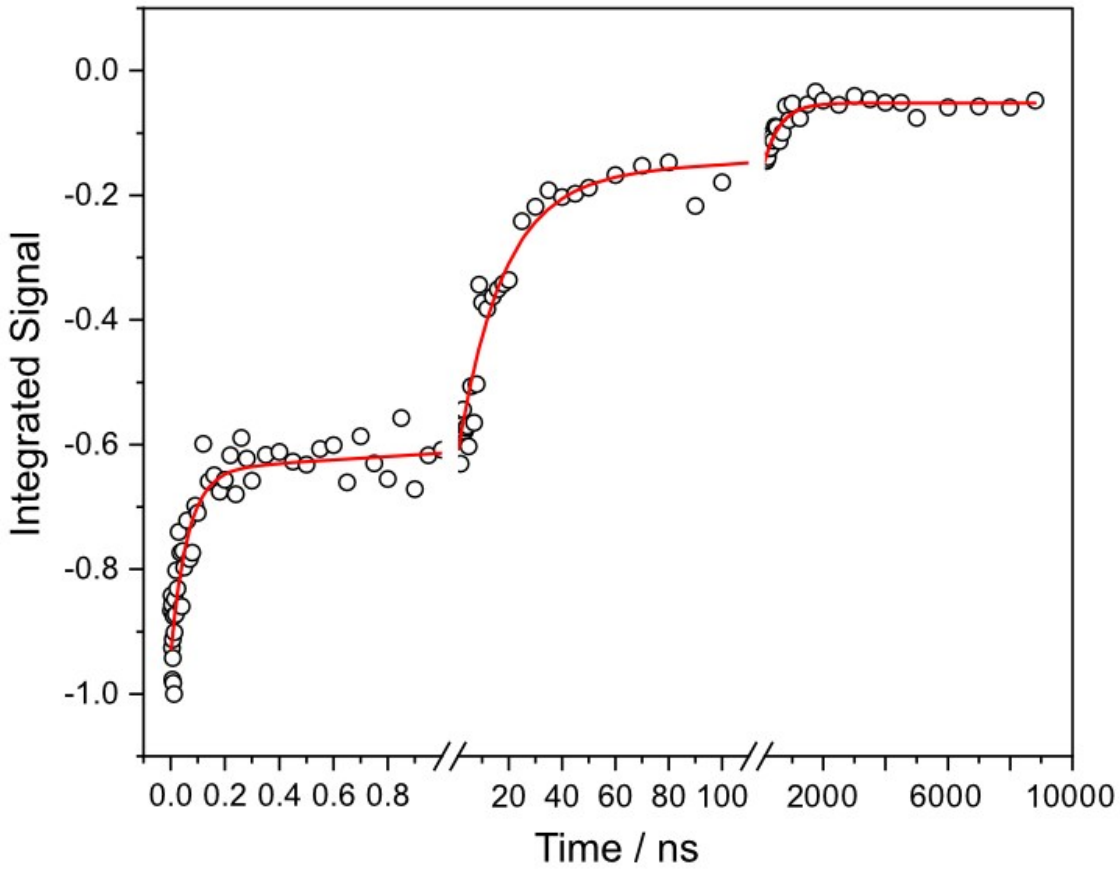

Figure S10. Kinetics of the loss of intensity of the ground state bleach centred at 1488 cm^{-1} at time delays from 100 ns to 9 µs. The solid line is a tri-exponential fit to the data, giving amplitudes $A_1 = 0.29 \pm 0.01$ $A_2 = 0.47 \pm 0.02$ $A_3 = 0.12 \pm 0.02$. The triplet quantum yield is calculated using $\Phi(T_1) = A_3/(A_1 + A_2 + A_3)$.

(v) PCBN with MBP in DMF

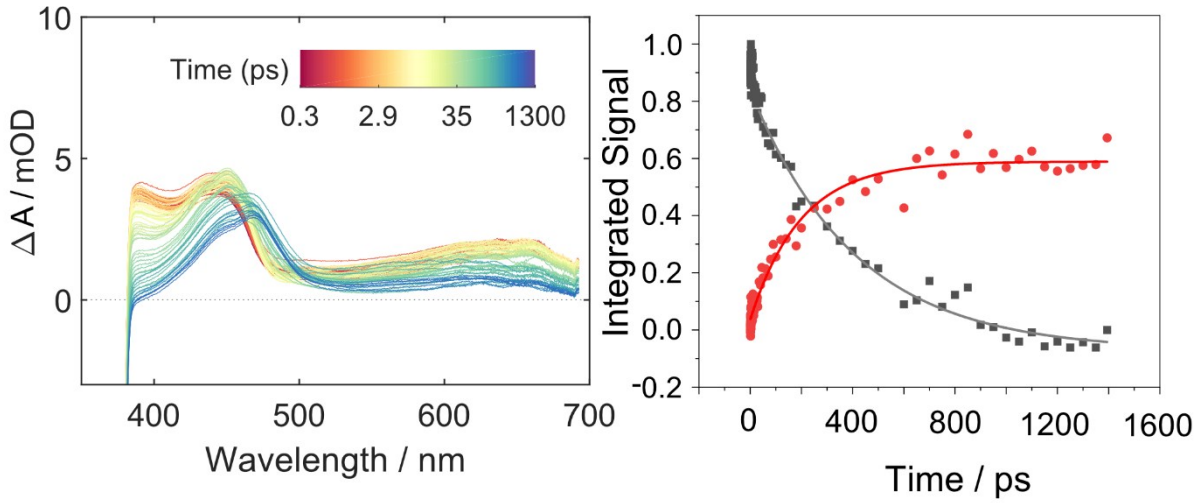

Figure S11. TEAS measurement over the wavelength range 350-700 nm following pulsed excitation of a PCBN and MBP solution in DMF at 370 nm. (a) TEA spectra for PCBN (2.1 mM) and MBP (1.17 M) in DMF (b) The corresponding kinetic traces obtained by spectral decomposition showing decay of the PCBN (S_1) absorption in grey and growth of the $PCBN^{\bullet+}$ (D_0) radical cation absorption in red.

(vi) PCBN TVAS in toluene-d_8

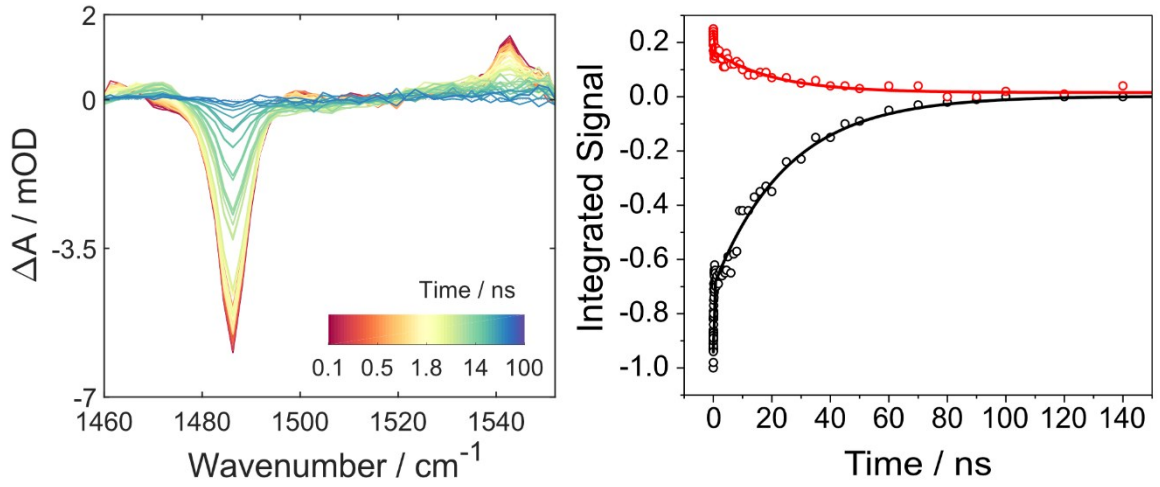

Figure S12. TVAS measurement over the wavenumber range 1460-1560 cm^{-1} following pulsed excitation of a PCBN / toluene-d_8 solution at 370 nm. (a) TVAS spectra for PCBN (2.1 mM) in toluene-d_8 from 1 ps to 100 ns (b) The corresponding kinetic traces obtained by spectral decomposition. Solid lines are global fits with biexponential time constants of τ_1 = 60 ± 7 ps and τ_2 = 25 ± 1 ns. Respective fit amplitudes of the GSB are A_1= 0.26 ± 0.01 and A_2 = 0.7 ± 0.01 . Note the full recovery of the GSB.

(vii) PCBN TVAS in DMF

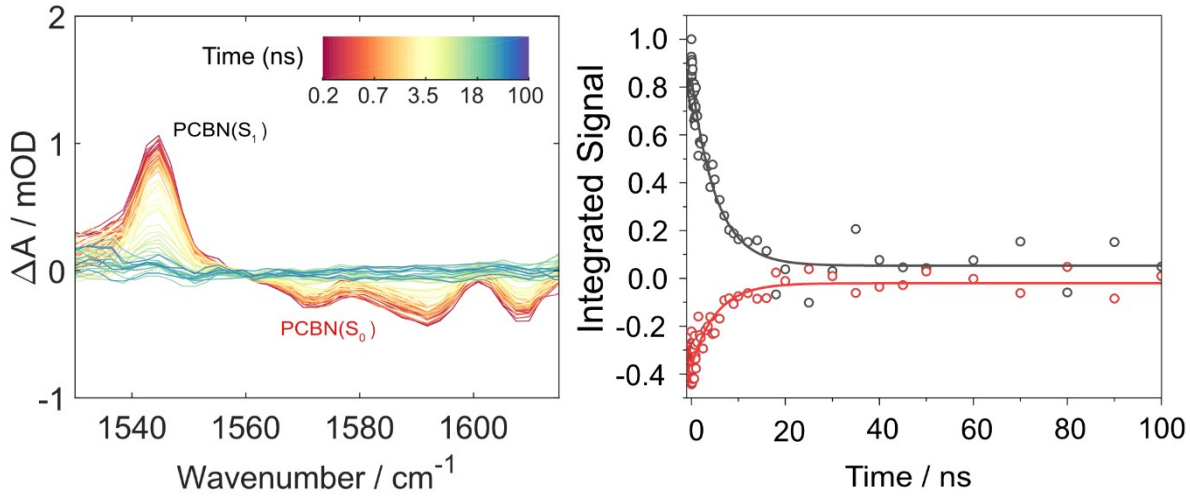

Figure S13. TVAS measurement over the wavenumber range 1530-1620 cm^{-1} following pulsed excitation of a PCBN / DMF solution at 370 nm. (a) TVAS spectra for PCBN (2.1 mM) in DMF from 1 ps to 100 ns (b) The corresponding kinetic traces obtained by spectral decomposition. Solid lines are global fits with single exponential time constants of τ_1=5.2 ± 0.4 ns. Note the full recovery of the GSB.

TEAS Data Fitting

(i) PCBN lifetime data

Figure S14 and **Figure S16** illustrate the methods we use to decompose transient electronic absorption spectra into spectral components with different kinetic behaviour in the KOALA program. An early time and a later time spectrum are chosen as basis functions to fit the time-evolving spectra, with examples shown in **Figure S14** and **Figure S16**. Although these two basis spectra are similar in form, spectral decomposition using a single basis function was unsuccessful. The

integrated intensities of these decaying and growing basis functions are plotted to obtain the kinetic traces shown in **Figure S7**, **Figure S8**, **Figure S9**, and **Figure S11**. **Figure S15(a)-S13(e)** show the progression of the fit using these basis functions at early, intermediate and later times, and the two basis spectra chosen provide a satisfactory account of transient spectra measured at all our experimental time delays. The close correspondence between time constants derived from kinetic fitting of the outcomes of this spectral decomposition and from analysis of time-resolved vibrational absorption spectroscopy data supports our choice of procedures.

The results of such an analysis of TEA spectra depends on the choice of basis functions. We therefore used SVD fitting in Glotaran software to test our chosen procedure further. This analysis supported use of two basis spectra similar to those chosen for use in KOALA, but suggested a weak component could arise from stimulated emission (most likely from the S_1 state, and weak because of the forbidden $S_1 - S_0$ transition). We therefore used the recorded fluorescence spectrum of PCBN as an additional basis function to account for a stimulated emission spectral component and found that the derived kinetics do not vary significantly from our decomposition without this component.

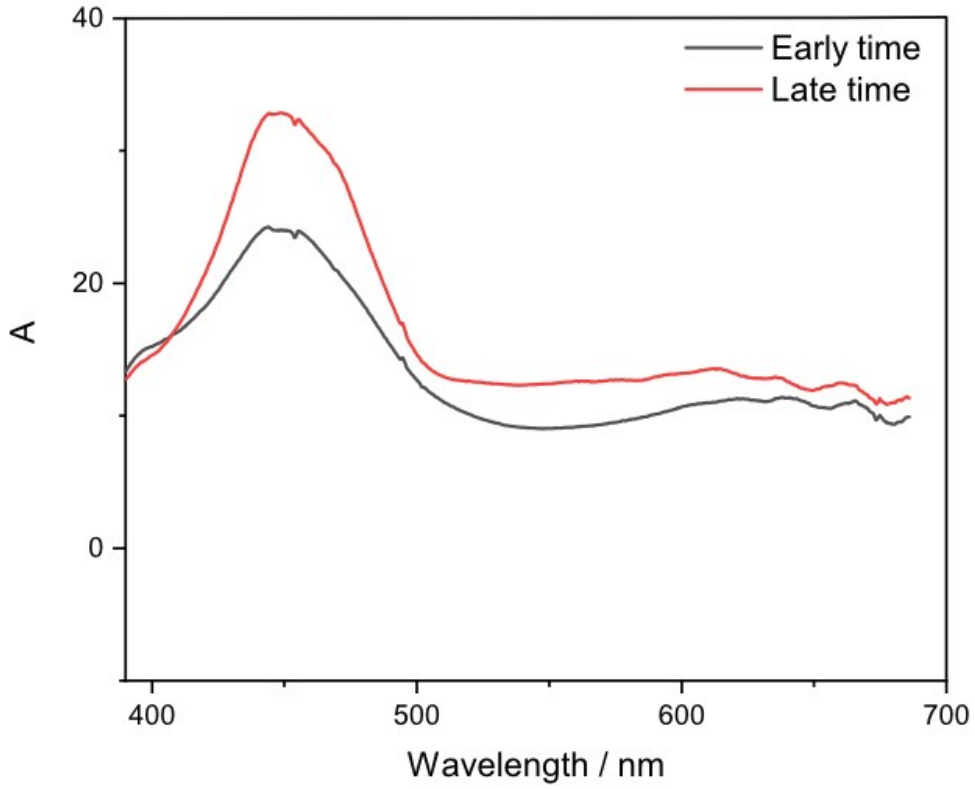

*Figure S14. Early (1 ps) and late (450 ps) time basis functions used for the decomposition of TEA spectra for PCBN in toluene, as shown in **Figure S7.** Although the two basis functions are similar in form, successful data analysis requires inclusion of both (see main text for further discussion). Subtle differences such as the broader 400 – 500 nm feature in the early time basis function likely reflect a combination of vibrational relaxation and internal conversion taking place between 1 ps and 450 ps.*

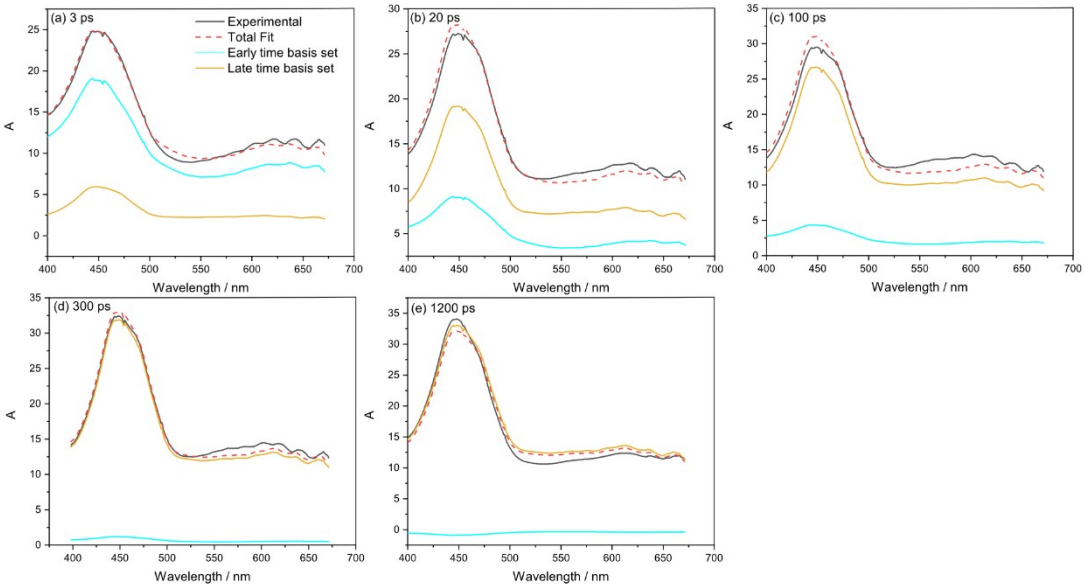

*Figure S15. Progression of the fit using the basis functions shown in **Figure S14** for PCBN in toluene at early (a and b), intermediate (c and d) and later times (e). Early and late time basis functions are represented by blue and yellow lines, respectively, the total fit is shown by the dashed red line, and the recorded spectra are plotted as solid black lines.*

(ii) PCBN and MBP data

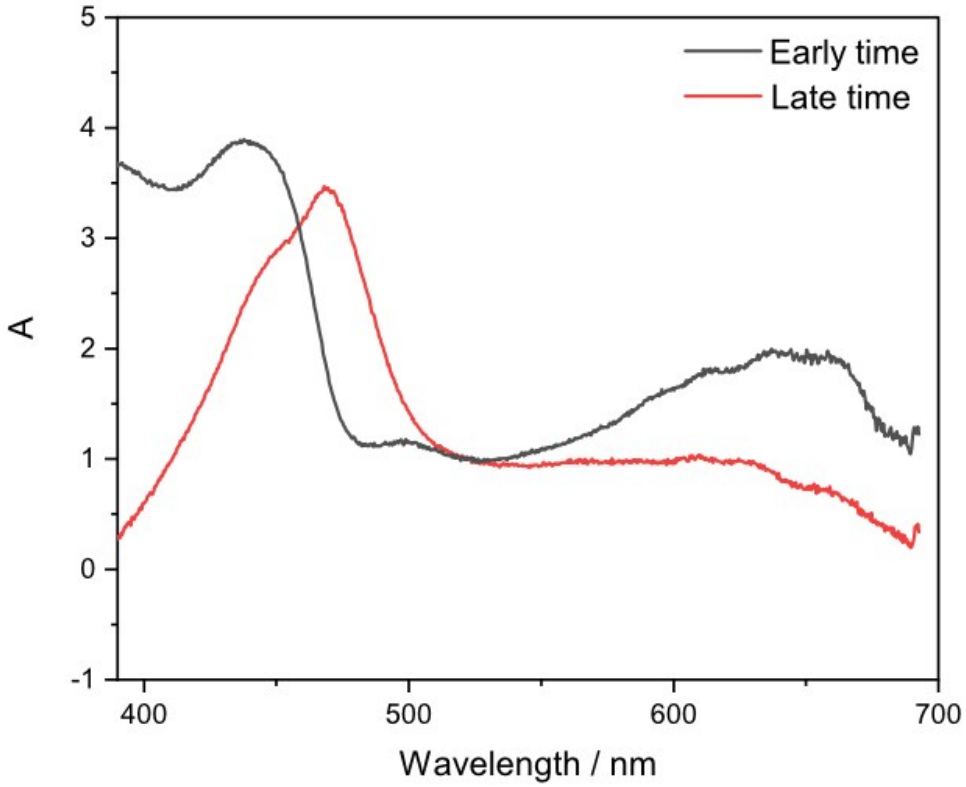

Figure S16. Early (1 ps, black) and late (1.3 ns, red) time basis functions used for the decomposition of TEA spectra for PCBN and MBP in DMF, as shown in ***Figure S11****.*

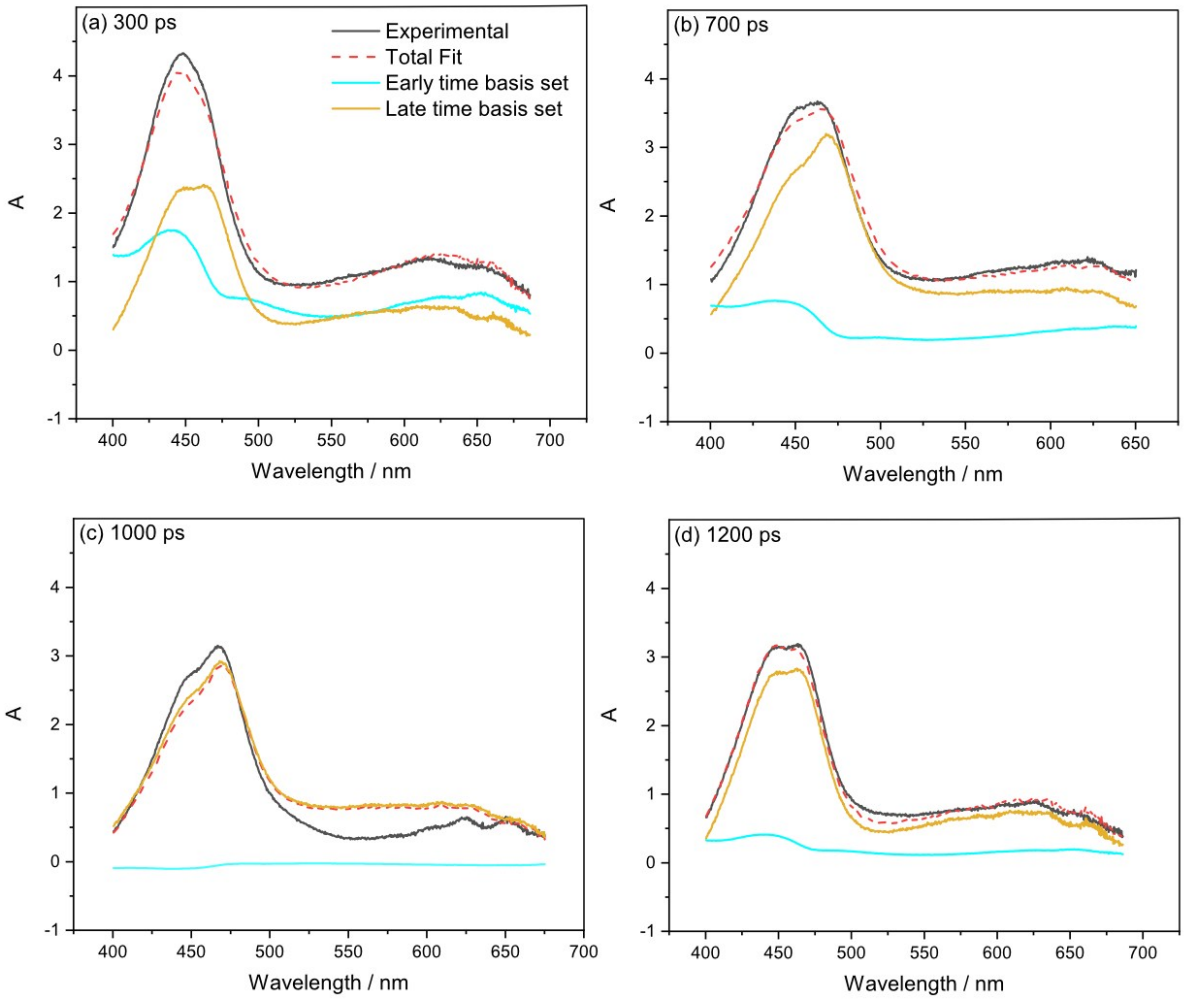

*Figure S17. Progression of the fit using the basis functions shown in **Figure S16** for PCBN and MBP in DMF at early (a), intermediate (b and c) and late (d) time delays. Early and late time basis functions are represented by blue and yellow lines, respectively, the total fit is shown by the dashed red line, and the recorded spectra are plotted as solid black lines.*

Kinetic Analysis

Kinetics of the electron transfer between photoexcited PCBN and MBP

(i) Kinetics for the rise of the $^2MP^{\bullet}(D_0)$ absorption band observed at 1660 cm^{-1} in TVA spectra obtained for a solution of PCBN (2.1 mM) and MBP (various concentrations from 0.2 - 1.1 M) in DCM following 370-nm excitation.

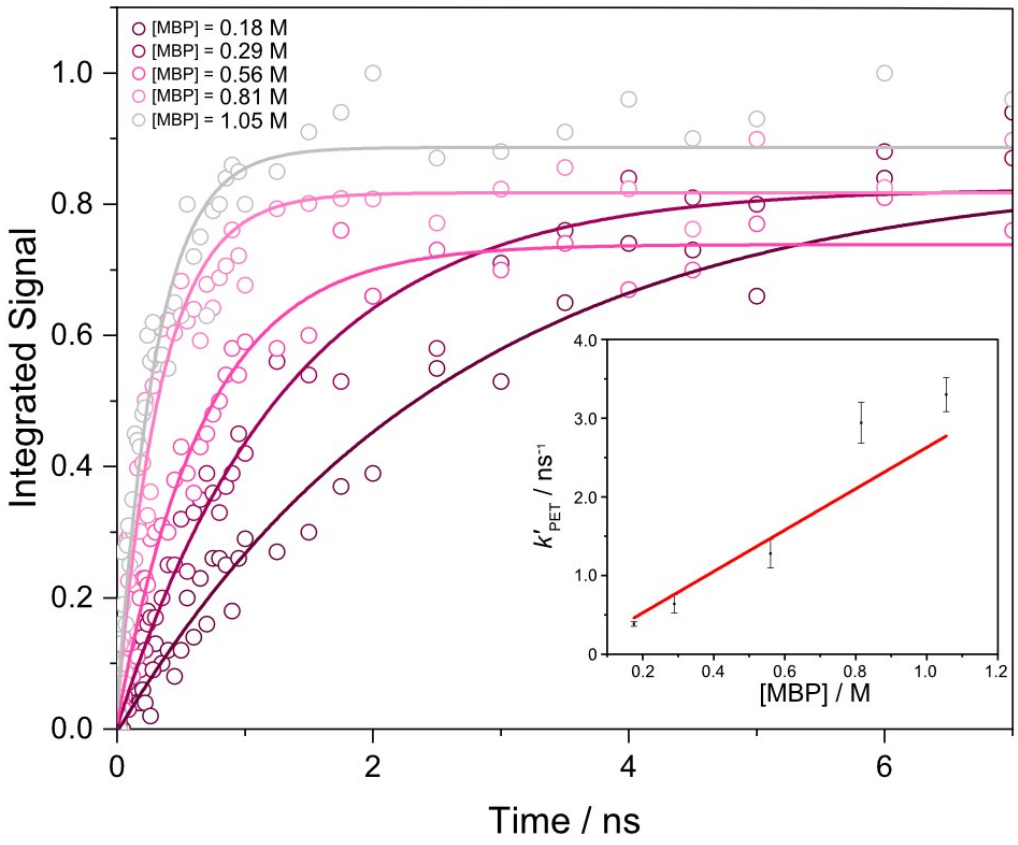

Figure S18. Kinetics of formation of $^2MP^{\bullet}(D_0)$ radicals by electron transfer from PCBN(S_1) to MBP in DCM. Each data set and fitted curve corresponds to a different concentration of MBP from 0.2 – 1.1 M. Solid lines are single exponential fits (see text for further discussion). First-order rate coefficients obtained from these fits are plotted against MBP concentration in the inset. The bimolecular rate coefficient for electron transfer is determined from the gradient of a linear fit to these points, weighted by the individual measurement errors, giving k_{PET} = (2.6 ± 0.3) × 10^9 dm^3 mol^{-1} s^{-1}. The diffusion limited rate coefficient in DCM is 1.6 x 10^{10} dm^3 mol^{-1} s^{-1} at 25 °C.[5]*

(ii) Kinetics for the rise of $^2MP^\bullet(D_0)$ absorption band observed at 1660 cm^{-1} in TVA spectra obtained for a solution of PCBN (2.1 mM) and MBP (various concentrations from 0.2 - 1.1 M) in toluene-d_8 following 370-nm excitation.

Figure S19. Kinetics of formation of $^2MP^{\bullet}(D_0)$ radicals by the electron transfer from PCBN(S_1) to MBP in toluene-d_8. Each data set and fitted curve correspond to a different concentration of MBP from 0.4 – 1.0 M. Solid lines are single exponential fits (see text for further discussion). First-order rate coefficients obtained from these fits are plotted against MBP concentration in the inset. The bimolecular rate coefficient for electron transfer is determined from the gradient of a linear fit to these points, weighted by the individual measurement errors, giving $k_{PET} = (3.1 \pm 0.1) \times 10^9$ dm^3 mol^{-1} s^{-1}. The diffusion limited rate coefficient in toluene is 1.2 x 10^{10} dm^3 mol^{-1} s^{-1} at 25 °C.[3]*

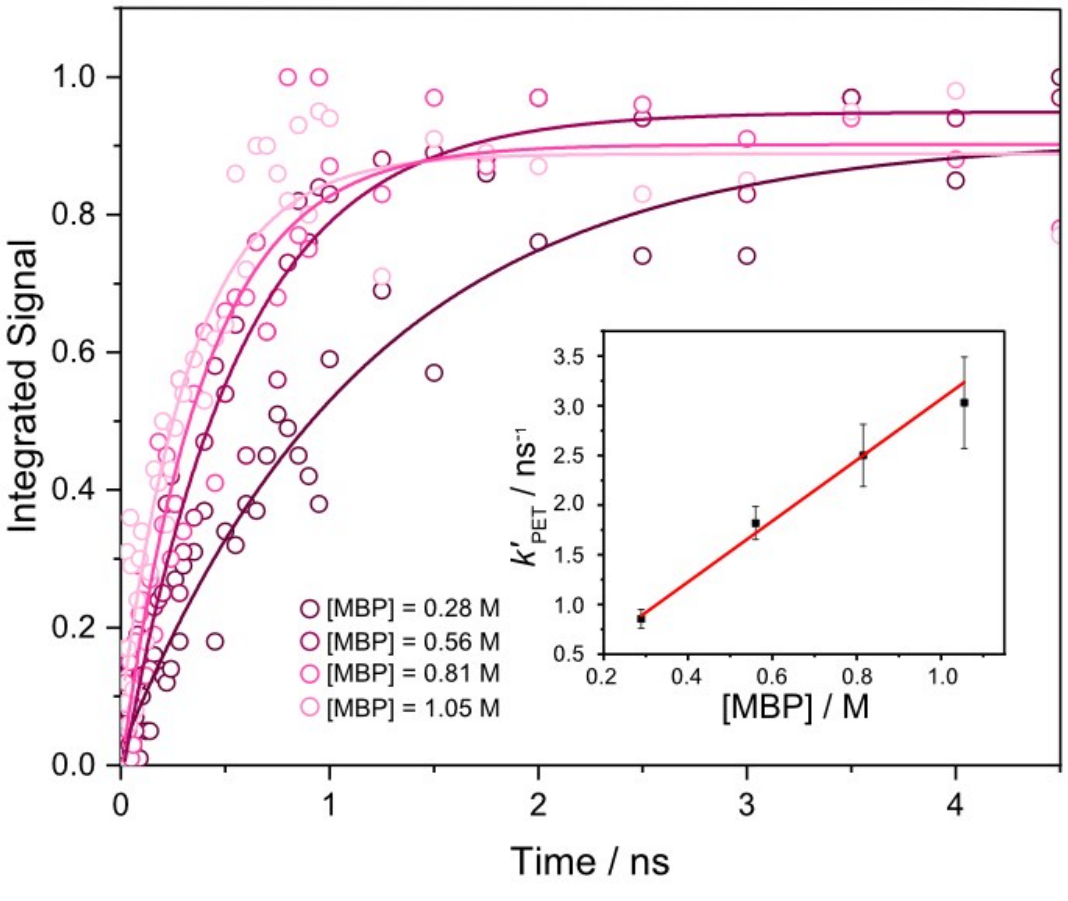

(iii) Kinetics of PCBN S_1 decay derived from analysis of TEA spectra obtained for a solution of PCBN (2.1 mM) and MBP (various concentrations from 0.2 – 1.1 M) in DMF following

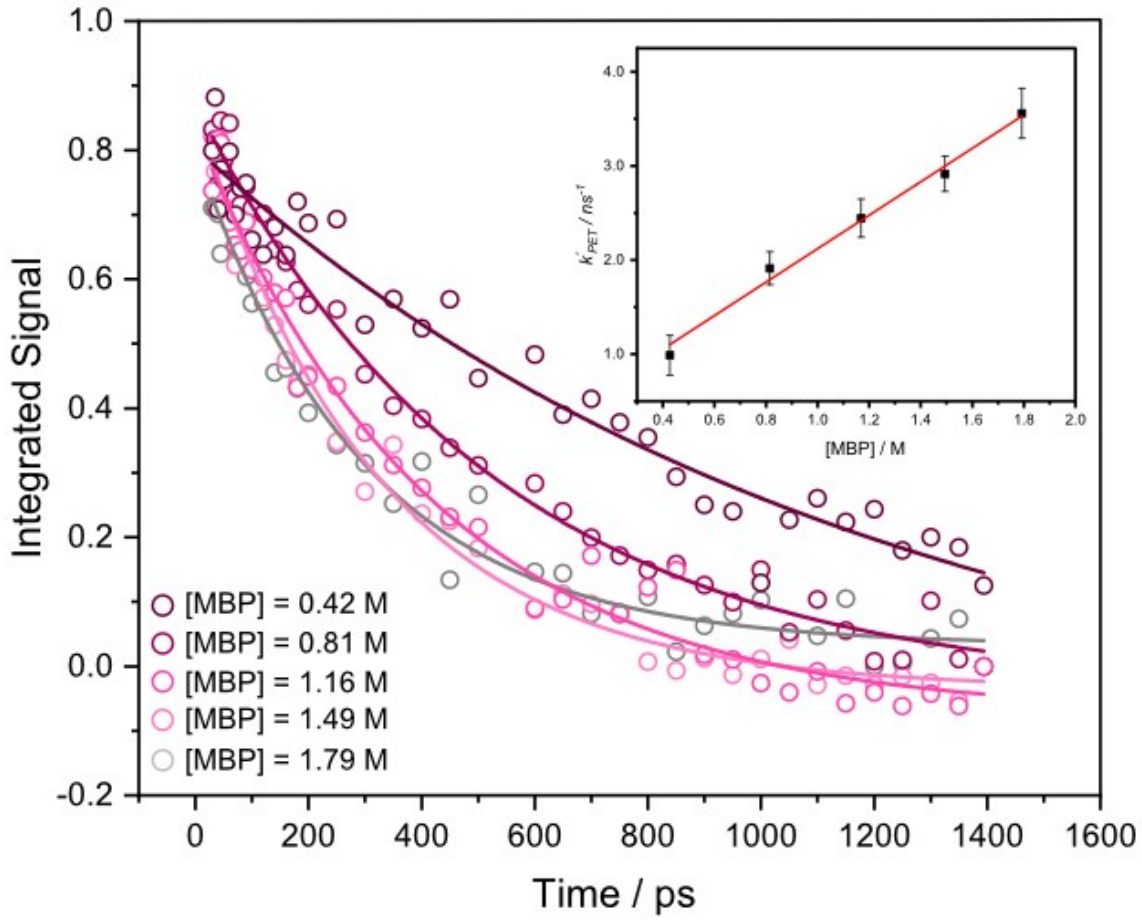

370-nm excitation

Figure S20. Rates of decay of $^1PC^*(S_1)$ by the electron transfer from $PCBN^*(S_1)$ (2.1 mM) to MBP in DMF. The $PC^*(S_1)$ state decays faster upon addition of MBP in increasing concentrations. Each data set and fitted curve correspond to an increased concentration of MBP from 0.4 – 1.8 M. Solid lines are single exponential fits. Rate constants obtained from these fits are plotted against MBP concentration in the inset. The rate constant for electron transfer is determined from the gradient of a linear fit to these points, weighted by the individual measurement errors, giving $k_{PET} = (1.8 \pm 0.1) \times 10^9$ dm^3 mol^{-1} s^{-1}. The intercept in the kinetic plot is 0.34 ± 0.13 ns^{-1} which corresponds to a decay lifetime in the absence of MBP of 2.9 ± 1.2 ns. This value is in reasonable agreement with the S_1 lifetime from TVAS data of 5.2 ± 0.4 ns. The kinetic model is explained in the text. The diffusion limited rate coefficient in DMF is 8.3 x 10^9 dm^3 $mol^{-1}s^{-1}$ at 25 °C.[5]

(iv) N_2 purged vs unpurged decay of the $^2MP^\bullet(D_0)$ absorption band observed at 1660 cm^{-1} in TVA spectra obtained for a solution of PCBN (2.1 mM) and MBP.

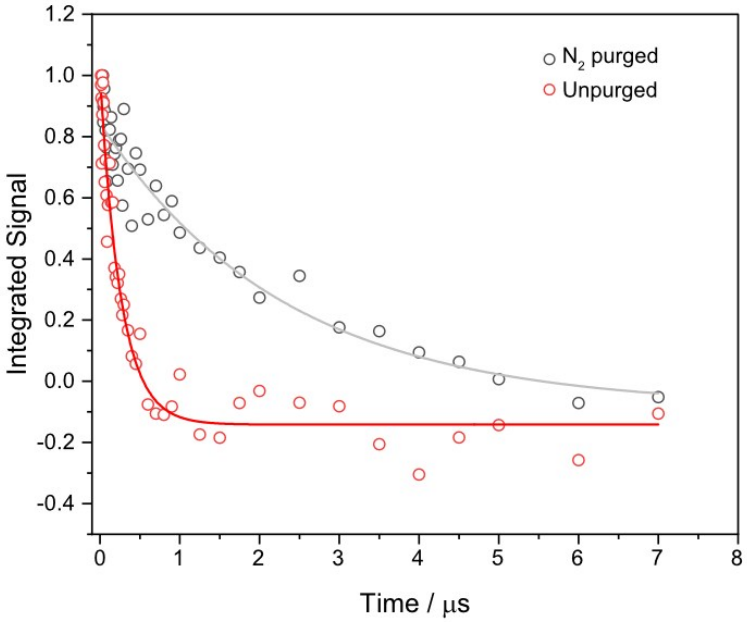

Figure S21. Rates of decay of $^2MP^\bullet(D_0)$ radicals in a N_2 purged vs unpurged system. Both data sets are for a solution of PCBN (4.2 mM) and MBP (0.2 M), either purged with N_2 for approximately 45 mins (grey) or not purged (red). The radical decays faster in an unpurged system where oxygen is present. Solid lines are single exponential fits and the corresponding time constants are τ = 2.3 ± 0.4 μs (N_2 purged) and τ = 260 ± 22 ns (unpurged).

Smoluchowski vs single exponential kinetic fitting

The electron transfer kinetics shown in **Figure S18**, **Figure S19**, and **Figure S20** arise from the reaction scheme shown below:

$$PCBN(S_1) + MBP \rightarrow PCBN^{+\bullet} + MP^\bullet + Br^-$$

We use a pseudo first-order analysis to fit the data as it can be assumed that $[PCBN(S_1)] \ll [MBP]$. The 1st-order kinetic scheme is represented as reactants converting to products:

$$R \rightarrow P$$

with a pseudo first-order rate coefficient *k* and a time constant $\tau = 1/k$. This pseudo first-order rate coefficient is the product of the bimolecular rate coefficient for reaction k_r and the concentration of the electron acceptor:

$$k = k_r[MBP] = k_r c_0$$

Here, c_0 denotes the initial (and excess) concentration of the electron acceptor. Neglecting diffusional effects, solution of the kinetic equation $d[R]/dt = -k[R]$ gives concentrations of R and P over time as:

$$[R]_t = [R]_0 \, exp(-kt) \qquad (1)$$

$$[P]_t = [R]_0 - [R]_t = [R]_0 \, (1 - exp(-kt)) \qquad (2)$$

Data in **Figure S18** and **Figure S19** have been fit with equation (2) and the values for k plotted against [MBP] to provide a value for k_r. However, this analysis does not account for the time-dependence of the rate coefficient as the reaction changes from the static limit to a diffusional limit.[6-8]

We can incorporate this additional complexity into the kinetic analysis by replacing equation (1) with:

$$[R]_t = [R]_0\, exp(-\int_0^t k(t')dt') \qquad (3)$$

where k is now a time-dependent pseudo-first order rate coefficient.

If there is also decay of the reactants (which are in an excited electronic state for photoredox catalysis) by fluorescence (with a fluorescence lifetime τ_f) equation (3) is modified to be:

$$[R]_t = [R]_0\, exp\left(-\int_0^t k(t')dt'\right) exp\left(-t/\tau_f\right) \qquad (4)$$

Smoluchowski theory assumes that reaction occurs instantaneously when the two reactants diffuse to some critical separation r. Under these approximations, the time-dependent rate coefficient takes the form:

$$k(t) = 4\pi D N_A r c_0 \left\{1 + \frac{r}{\sqrt{\pi D t}}\right\} \qquad (5)$$

Where N_A is the Avogadro constant, and D is the sum of the diffusion coefficients for the two reactants. Equation (5) is readily integrated with respect to time:

$$\int_0^t k(t')dt' = 4\pi D N_A r c_0 \left\{t + \frac{2r\sqrt{t}}{\sqrt{\pi D}}\right\} \qquad (6)$$

Inserting this result into equation (4) gives:

$$[R]_t = [R]_0\, exp\left(-4\pi D N_A r c_0 \left\{t + \frac{2r\sqrt{t}}{\sqrt{\pi D}}\right\}\right) exp\left(-t/\tau_f\right) \qquad (7)$$

In these expressions, $4\pi D N_A r = k_D$ which is the bimolecular diffusion rate coefficient. Here, we treat it as a second-order rate coefficient, k_r, approaching the diffusional limit. This approach approximates the more complete Smoluchowski-Collins-Kimball (SCK) treatment[7-9] but our data do not merit the more involved fitting required by SCK theory. The functional form of equation (7), or of the corresponding expression for growth of products, is implemented in fits using Origin software to obtain $k' = k_r c_0$ values which can be plotted against c_0 to extract a value for k_r from a linear fit. In the fits, we fix τ_f to be either the S_1 state lifetime of PCBN in the absence of MBP (17 ns) or a larger value. Either approach gives the same outcome.

This fitting procedure is exemplified by re-analysis of the data presented in **Figure S18** for the rise of the ^{2}MP$^\bullet$(D_0) absorption band at different initial concentrations of MBP. The Smoluchowksi model fitting is shown in **Figure S22** in which each data set has been fitted to $\{[R]_0 - [R]_t\}$ with $[R]_t$ given by **equation 7**. The inset shows the linear dependence of extracted *k'* values on c_0 = [MBP]. The rate

coefficient obtained from this analysis is (2.3 ± 0.1) x 10^9 dm^3 mol^{-1} s^{-1}, which agrees within the mutual uncertainties of those derived from single exponential fits. The agreement suggests that static quenching does not make a major contribution to the electron transfer reaction kinetics at these concentrations.

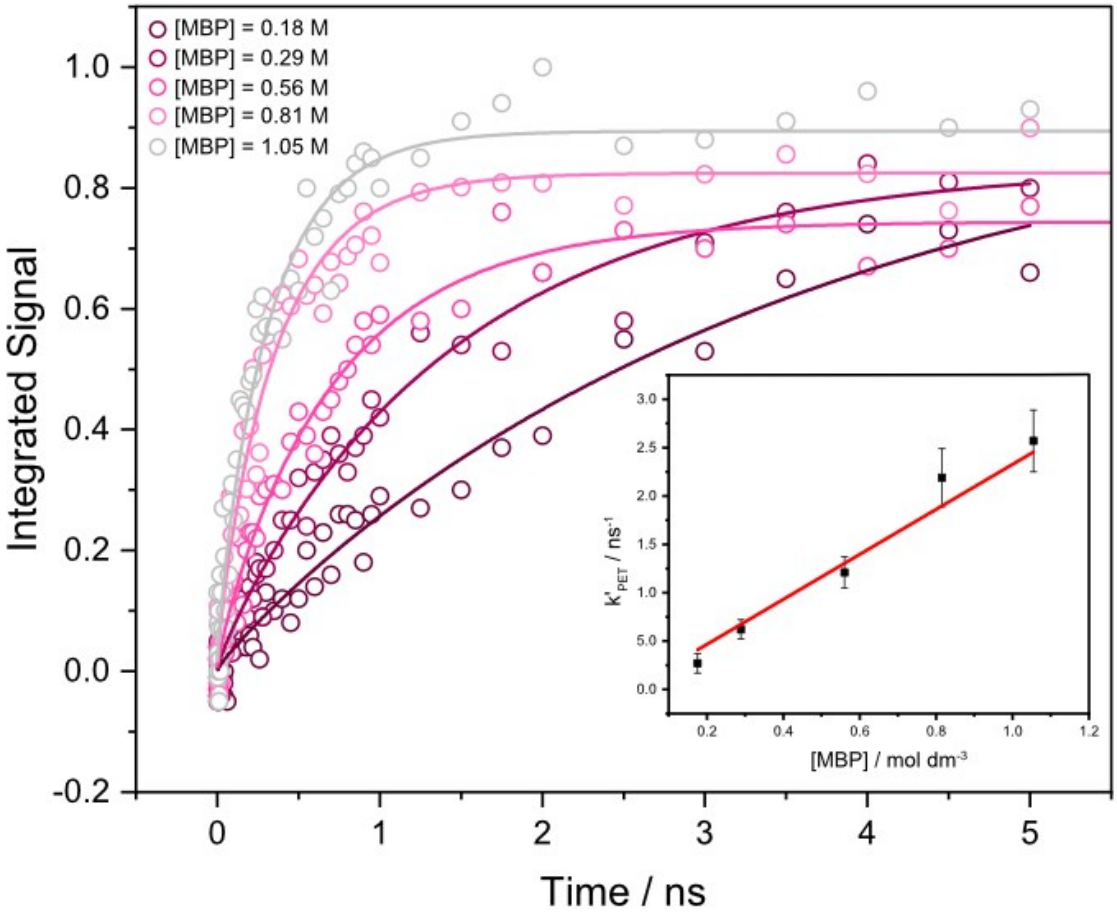

Figure S22. Kinetics of formation of $^2MP^{\bullet}(D_0)$ radicals by electron transfer from PCBN(S_1) to MBP in DCM. Each data set and fitted curve correspond to a different concentration of MBP from 0.2 – 1.1 M. Solid lines are fits using the Smoluchowski model described in the main text. The resulting pseudo-first order rate coefficient values are plotted against MBP concentration in the inset and a linear fit (weighted by the measurement uncertainties) gives the bimolecular rate coefficient for electron transfer k_{PET} = (2.3 ± 0.1) × 10^9 dm^3 mol^{-1} s^{-1}. This is almost an order of magnitude lower than the expected diffusional rate coefficient k_D = 1.6 × 10^{10} dm^3 mol^{-1} s^{-1} in DCM at 25 °C.[5]*

Calculations for $\Delta(\Delta_{PET}G)$

Photocatalyst	PC(S_1) Gibbs energy / kJ mol^{-1}	Radical cation Gibbs energy / kJ mol^{-1}	ΔG / kJ mol^{-1}
PCH	249	18	-231
PCF	213	28	-185
PCBN	204	22	-182

Table 1 Values used for the calculation of Δ($\Delta_{PET}G$)

$$\Delta_{PET}G = F\{E^0\left(PC^{+\bullet}/PC\right) - E^0(RX/R^{\cdot}X^{-})\} - E(PC^{*}(S_1)) - w$$

$$\Delta(\Delta_{PET}G) = F\{E^0(PC_A{}^{*}(S_1)/PC_A{}^{+\bullet}) - E^0(PC_B{}^{*}(S_1)/PC_B{}^{+\bullet})\}$$

$$\Delta(\Delta_{PET}G)(PCH/PCF) = \Delta_{PET}G(PCH) - \Delta_{PET}G\,(PCF) = -46\ kJ\ mol^{-1}$$

$$\Delta(\Delta_{PET}G)(PCH/PCBN) = \Delta_{PET}G(PCH) - \Delta_{PET}G\,(PCBN) = -49\ kJ\ mol^{-1}$$

$$\Delta(\Delta_{PET}G)(PCF/PCBN) = \Delta_{PET}G(PCF) - \Delta_{PET}G\,(PCBN) = -3\ kJ\ mol^{-1}$$

The Gibbs energies of the PC S_1 states are estimated from the maxima in the experimental emission spectra: PCBN[λ^{e}_{max}(DCM) = 587 nm, 204 kJ mol^{-1}]; PCF[λ^{e}_{max}(DCM) = 562 nm, 213 kJ mol^{-1}]; and PCH[[λ^{e}_{max}(DCM) = 480 nm, 249 kJ mol^{-1}]. The radical cation Gibbs energies are calculated from experimentally determined redox potentials.[2]

Kinetic Models

(i) Kinetic model for PCBN* / MBP electron transfer reactions for the analysis of PCBN*(S_1) decay rates

The decay of the PCBN excited state in the presence of MBP has two pathways corresponding to either relaxation to the ground state (radiative and non-radiative, with total unimolecular rate coefficient k_d) or by photoinduced electron transfer (with bimolecular rate coefficient k_{PET}). We take this competition into account when analysing the TEAS data for the decay of the PCBN* excited state absorption (ESA) through the kinetic model derived below:

$$\frac{d[PCBN^*]}{dt} = -k_d[PCBN^*] - k_{PET}[MBP][PCBN^*]$$

$$= -[PCBN^*](k_d + k_{PET}[MBP])$$

$$= -k_{obs}[PCBN^*]$$

$$k_{obs} = k_d + k_{PET}[MBP]$$

An exponential fit to time-dependent ESA band intensities gives rate coefficients k_{obs} for each [MBP]. A linear fit to a plot of k_{obs} against [MBP] then gives k_d from the intercept and k_{PET} from the gradient.

(ii) Kinetic model for the propagation reaction step

The presence of dissolved oxygen in the system introduces a pathway for MP$^{\bullet}$ decay which competes with reaction with isoprene, as is shown in **Figure S23**. The MP$^{\bullet}$ + MP$^{\bullet}$ termination reaction is not significant under our conditions because the concentration of MP$^{\bullet}$ is always considerably less than that of the isoprene monomer or dissolved oxygen. This reasoning is confirmed by experimental measurements in the absence of isoprene and following careful removal of dissolved oxygen by nitrogen purging, with a positive nitrogen pressure to prevent further influx of air. Under these conditions, the MP$^{\bullet}$ radical decay time is measured to be ~3 µs, compared to 300 ns for an unpurged solution.

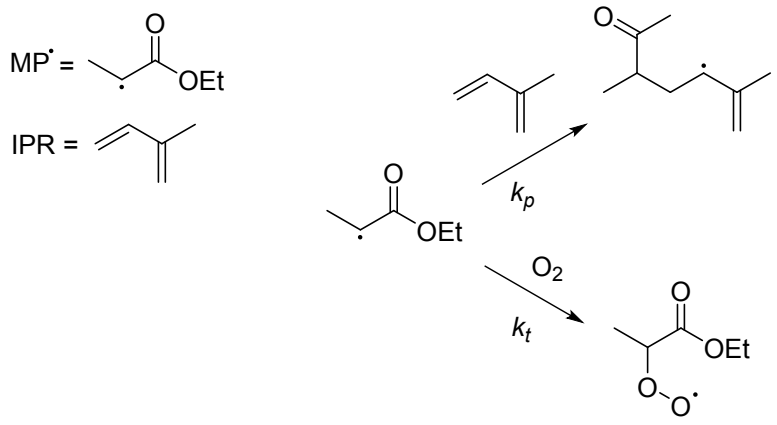

Figure S23. Competing pathways for the decay of MP• by reaction with the monomer isoprene (with propagation rate coefficient k_p) or with dissolved oxygen (with termination rate coefficient k_t).

This competitive loss of MP• radicals is considered when fitting the data for decay of the MP• absorption using the kinetic model derived below. In this model, isoprene is abbreviated to IPR.

$$\frac{d[MP^\bullet]}{dt} = -k_p[MP^\bullet][IPR] - k_t[MP^\bullet][O_2]$$

Under our conditions of $[O_2]$, [IPR] >> [MP•]:

$$\frac{d[MP^\bullet]}{dt} = -(k'_p + k'_t)[MP^\bullet]$$

With pseudo-first order rate coefficients:

$$k'_p = k_p[IPR]$$

$$k'_t = k_t[O_2]$$

An exponential fit to a data set of [MP•] vs. time gives a rate coefficient $k = k'_p + k'_t$ for each [IPR]. A linear fit to a plot of $k = k'_p + k'_t$ vs [IPR] then gives k_p from the gradient. Our N_2 purging of solutions minimizes the contribution of the O_2 reaction to the MP• radical loss so that the experimental data mostly reflect loss by reaction with IPR.

Computational Methodology

Excited State Calculations

The first excited singlet states and frontier molecular orbitals of the excited states of PCBN were computed using time-dependent density functional theory (TD-DFT) methods[10] at the CAM-B3LYP/6-31+G(d)/SCRF=(SMD, DCM) level of theory. CAM-B3LYP was chosen because it is reported to account successfully for the charge separation observed in the excited states of excited organic dyes.[11, 12] All calculations were performed using the Gaussian 09 software package.[13]

Excited State	Transition wavelength / nm	Oscillator strength
S_1	379	0.0025
S_2	378	0
S_3	358	0
S_4	315	0.2344

References

1. J. C. Theriot, C.-H. Lim, H. Yang, M. D. Ryan, C. B. Musgrave and G. M. Miyake, *Science*, 2016, **352**, 1082-1086.
2. M. P. Grubb, A. J. Orr-Ewing and M. N. R. Ashfold, *Rev. Sci. Instrum.*, 2014, **85**, 064104.
3. G. M. Greetham, D. Sole, I. P. Clark, A. W. Parker, M. R. Pollard and M. Towrie, 2012, **83**, 103107.
4. G. M. Greetham, P. M. Donaldson, C. Nation, I. V. Sazanovich, I. P. Clark, D. J. Shaw, A. W. Parker and M. Towrie, *Appl. Spectrosc.*, 2016, **70**, 645-653.
5. A. C. Marco Montalti, Luca Prodi, M. Teresa Gandolfi, *Handbook of Photochemistry*, Taylor & Francis Group, Boca Raton, FL, Third edn., 2006.
6. T. Kumpulainen, B. Lang, A. Rosspeintner and E. Vauthey, *Chem. Rev.*, 2017, **117**, 10826-10939.
7. D. D. Eads, B. G. Dismer and G. R. Fleming, *J. Chem. Phys.*, 1990, **93**, 1136-1148.
8. M. Rini, D. Pines, B.-Z. Magnes, E. Pines and E. T. J. Nibbering, *J. Chem. Phys.*, 2004, **121**, 9593-9610.
9. F. C. Collins and G. E. Kimball, *J. Colloid Sci.*, 1949, **4**, 425-437.
10. C. Adamo and D. Jacquemin, *Chem. Soc. Rev.*, 2013, **42**, 845-856.
11. T. Yanai, D. P. Tew and N. C. Handy, *Chem. Phys. Lett.*, 2004, **393**, 51-57.
12. M. J. G. Peach, P. Benfield, T. Helgaker and D. J. Tozer, *J. Chem. Phys.*, 2008, **128**, 044118.
13. M. J. T. Frisch, G. W.; Schlegel, H. B.; Scuseria, G. E.; Robb, M. A.; Cheeseman, J. R.; Scalmani, G.; Barone, V.; Mennucci, B.; Petersson, G. A.; Nakatsuji, H.; Caricato, M.; Li, X.; Hratchian, H. P.; Izmaylov, A. F.; Bloino, J.; Zheng, G.; Sonnenberg, J. L.; Hada, M.; Ehara, M.; Toyota, K.; Fukuda, R.; Hasegawa, J.; Ishida, M.; Nakajima, T.; Honda, Y.; Kitao, O.; Nakai, H.; Vreven, T.; Montgomery, J. A.; Peralta, J. E.; Ogliaro, F.; Bearpark, M. J.; Heyd, J. J.; Brothers, E.; Kudin, K. N.; Staroverov, V. N.; Kobayashi, R.; Normand, J.; Raghavachari, K.; Rendell, A.; Burant, J. C.; Iyengar, S. S.; Tomasi, J.; Cossi, M.; Rega, N.; Millam, J. M.; Klene, M.; Knox, J. E.; Cross, J. B.; Bakken, V.; Adamo, C.; Jaramillo, J.; Gomperts, R.; Stratmann, R. E.; Yazyev, O.; Austin, A. J.; Cammi, R.; Pomelli, C.; Ochterski, J. W.; Martin, R. L.; Morokuma, K.; Zakrzewski, V. G.; Voth, G. A.; Salvador, P.; Dannenberg, J. J.; Dapprich, S.; Daniels, A. D.; Farkas, O.; Foresman, J. B.; Ortiz,J. V.; Cioslowski, J.; Fox, D. J. , *Gaussian 09, Gaussian Inc., Wallingford CT*, 2009.